Int. J. Heat Mass Transfer. Vol. 35, No. 5, pp. 1131–1141, 1992
Printed in Great Britain

0017–9310/92 $5.00 + 0.00

Rigorous numerical solutions and correlations for two-dimensional laminar buoyant jets

W. S. YU, H. T. LIN† and H. C. SHIH
Department of Chemical Engineering, National Central University, Chungli, Taiwan 32054, Republic of China

(*Received* 5 *February* 1991 *and in final form* 17 *May* 1991)

Abstract—A very effective and accurate solution method is proposed for studying the free and the wall buoyant jets. The buoyant jets are treated as a combined system of the momentum jets and buoyant plumes, and are analyzed by introducing some dimensionless variables of proper scales over the entire range of buoyancy. An effective and rigorous finite difference scheme is developed to solve the nonsimilar equations subject to the integral constraints of momentum and heat flow conservations. Very accurate correlation equations are proposed for predicting the centerline temperature and the centerline velocity of the two-dimensional laminar free buoyant jets. Correlations of the surface temperature and the surface shear stress of the wall buoyant jets are also presented.

1. INTRODUCTION

HOT FLUID discharged from a narrow slot into a large quiescent fluid reservoir of lower temperature is termed a plane (or two-dimensional) buoyant jet. Both the unconfined free jet and the wall jet propagating tangentially along a flat surface have been studied [1–16]. The flow and thermal characteristics of buoyant jets are of great interest in many industrial systems and some environmental studies, such as mixing, ocean circulations, and air or water pollution, etc. In practice, the jet flow is turbulent and most of the previous investigations deal with turbulent buoyant jets. However, laminar jets have also been studied extensively [1–16], since turbulent jets can be analyzed mathematically in an identical way [17] except that an empirical constant has to be determined experimentally.

It is known [7, 8] that the buoyant jet behaves like a pure momentum jet at the region near the nozzle, at which the buoyancy force is negligible when compared with the inertia force. In the downstream region far from the nozzle, where the buoyancy force is dominant, the buoyant jet is equivalent to a buoyant plume arising from a line heat source. The limiting cases of pure momentum jets and pure buoyant plumes have been investigated by many researchers [1–5, 18–20].

For the past two decades, the research on laminar jets has concentrated on the effects of buoyancy [7–15]. However, most of the previous analyses do not cover the entire range of buoyancy intensity. Starting from one of the quite different scaling laws of the two limiting cases, the previous solutions are valid only for the region near or far from the slit. Accurate solutions and correlations are not available for the intermediate region where the inertia is comparable with buoyancy.

In this paper, we introduce new buoyancy parameters and transformation variables that are of proper scaling laws for the jet, plume, and transition regions. The obtained universal formulations of buoyant jets can be readily reduced to the self-similar equations of pure momentum jets and to those of pure buoyant plumes. We have also developed a very effective finite difference scheme to solve the set of nonsimilar equations subjected to the boundary conditions and the additional two integral constraints of momentum and heat flux conservations. The numerical method is very useful for studying other complicated systems of jets and plumes.

The proper dimensionless variables, the universal formulations, and the effective numerical scheme resulted in very accurate solutions for the buoyant jets over the entire region of buoyancy. In addition, simple but very accurate correlation equations of the centerline temperature and the centerline velocity of the free buoyant jet, as well as the surface temperature and the surface friction of the wall buoyant jet, can be derived in terms of the values of the pure momentum jet and the pure buoyant plume.

2. ANALYSIS

2.1. *System descriptions and governing equations*

We consider laminar, plane buoyant jets of incompressible fluid emerging vertically from a long, narrow slit of width w and spreading into a quiescent fluid reservoir of a constant temperature T_∞. For the free jet the flow is unconfined after discharging from the slit, while for the wall jet the flow develops tangentially along an adiabatic vertical flat plate. According to the Boussinesq and boundary-layer approximations, the governing equations of the plane buoyant jets are

$$\frac{\partial u}{\partial x}+\frac{\partial v}{\partial y}=0 \tag{1}$$

$$u\frac{\partial u}{\partial x}+v\frac{\partial u}{\partial y}=\nu\frac{\partial^2 u}{\partial y^2}\pm g\beta(T-T_\infty) \tag{2}$$

† To whom correspondence should be addressed.

NOMENCLATURE

A, B, C defined in equation (46)
c_p specific heat
C_f friction coefficient, $\tau_s/\rho(v/x)^2$
f dimensionless stream function
F $\int_0^\infty f'f'\,d\eta$
g gravitational acceleration
G $\int_0^\infty \theta\,d\eta$
Gr local Grashof number, $g\beta|T^*|x^3/v^2$
Gr_w Grashof number based on the width of the slit, $g\beta|T^*|w^3/v^2$
H $\int_0^\infty f'\theta\,d\eta$
J_0 initial momentum of the jet per unit length of source
Pr Prandtl number, v/α
Q_0 heat flow per unit length of source
Re local Reynolds number, u_0x/v
Re_w Reynolds number based on the width of the slit, u_0w/v
T temperature
T^* characteristic temperature, $Q_0/\rho c_p v$
u, v longitudinal and transverse components of velocity
u_0 mean initial velocity of the jet
U dimensionless longitudinal velocity, $(u/u_0)(Re_w^2/Gr_w)^{1/4}$ for the free jet, and $(u/u_0)(Re_w^2/Gr_w)^{2/7}$ for the wall jet
w width of the slit
x, y longitudinal and transverse coordinates, respectively
X, Y dimensionless longitudinal and transverse coordinates.

Greek symbols
α thermal diffusivity
β thermal expansion coefficient
ζ buoyancy parameter, equation (17)
η dimensionless transverse coordinate, $(y/x)\lambda$
θ dimensionless temperature, $(T-T_\infty)\lambda/T^*$
λ unified scale parameter, equation (13)
v kinematic viscosity
ξ dimensionless longitudinal coordinate, $(1+\zeta)^{-1}$
ρ density of fluid
τ shear stress
φ dimensionless temperature, $[(T-T_\infty)/T^*](Re_w^6/Gr_w)^{1/4}$ for the free jet, and $[(T-T_\infty)/T^*](Re_w^9/Gr_w)^{1/7}$ for the wall jet
ψ stream function.

Subscripts
c at the centerline of the free jet
i ith iteration
j at transverse position level j
s on the surface of the flat plate
0 initial value of the jet
∞ of the ambient fluid.

Superscripts
$'$ partial derivative with respect to η
n at longitudinal position level n.

$$u\frac{\partial T}{\partial x}+v\frac{\partial T}{\partial y}=\alpha\frac{\partial^2 T}{\partial y^2}. \tag{3}$$

The axial distance x is measured from a virtual line source of heat and momentum [10, 13]. The plus sign in front of the last term of equation (2) represents the buoyancy assisting flow, i.e. the case of hot fluid ejected upward or cold fluid downward. The minus sign denotes the case of buoyancy opposing flow. The associated boundary conditions are

at $y=0$: $v=0,\quad \partial T/\partial y=0$ (4)

$\partial u/\partial y=0$ for a free jet (5a)

$u=0$ for a wall jet (5b)

as $y\to\infty$: $u=0,\quad T=T_\infty$. (6)

2.2. *The integral constraints*

In addition to the above boundary conditions, two integral constraints should be considered to obtain nontrivial solutions. The first constraint is derived through the integration of the momentum equation (2) across the flow field:

$$\frac{d}{dx}\int_{-\infty}^{\infty}u^2\,dy=\int_{-\infty}^{\infty}g\beta(T-T_\infty)\,dy \quad \text{for a free jet} \tag{7a}$$

and

$$\frac{d}{dx}\left[\int_0^\infty u\left(\int_y^\infty u^2\,dy\right)dy\right]=\int_0^\infty u\left[\int_y^\infty g\beta(T-T_\infty)\,dy\right]dy \quad \text{for a wall jet.} \tag{7b}$$

At the region very close to the slit nozzle ($x\to 0$), the buoyancy force is negligible and the jets are non-buoyant. Therefore, the initial conditions of equations (7a) and (7b) can be obtained, respectively, as

$$J_0=\lim_{x\to 0}\int_{-\infty}^{\infty}\rho u^2\,dy=\text{constant} \quad \text{for a free jet} \tag{8a}$$

and

$$K_0 = \lim_{x\to 0}\int_0^\infty \rho u\left(\int_y^\infty \rho u^2\,\mathrm{d}y\right)\mathrm{d}y = \text{constant}$$

for a wall jet. (8b)

Another constraint comes from energy conservation. The energy carried by the boundary-layer flow, across the half plane at any $x > 0$, is constant and equal to the energy released from the slit. Hence

$$\rho c_p\int_0^\infty u(T-T_\infty)\,\mathrm{d}y = \begin{cases} Q_0/2 & \text{for a free jet} \quad (9a)\\ Q_0 & \text{for a wall jet} \quad (9b)\end{cases}$$

where Q_0 is the rate of heat flow discharged from the slit per unit length. By introducing the mean initial velocity of the jets as

$$u_0 = (J_0/\rho w)^{1/2} \quad \text{for a free jet} \qquad (10a)$$

or

$$u_0 = (2K_0/\rho^2 w^2)^{1/3} \quad \text{for a wall jet} \qquad (10b)$$

the quantity Q_0 can be expressed in terms of the initial values u_0 and T_0 of the jet:

$$Q_0 = \rho c_p u_0 w(T_0 - T_\infty). \qquad (11)$$

2.3. *Transformation variables*

To facilitate the numerical computations, a non-similar transformation based on some novel transformation variables is accomplished. The proposed dimensionless transverse coordinate is

$$\eta = (y/x)\lambda \qquad (12)$$

with the unified scale parameter λ defined by

$$\lambda = (Re_w\, Re)^{1/3} + Gr^{1/5} \quad \text{for a free jet} \qquad (13a)$$

or

$$\lambda = (Re_w^2\, Re)^{1/4} + Gr^{1/5} \quad \text{for a wall jet} \qquad (13b)$$

where

$$Re = u_0 x/\nu \quad \text{and} \quad Re_w = u_0 w/\nu \qquad (14)$$

are the local Reynolds number and the Reynolds number based on the width of the slit, respectively. The local Grashof number is defined as

$$Gr = g\beta|T^*|x^3/\nu^2 \qquad (15)$$

where

$$T^* = Q_0/(\rho c_p \nu) = (T_0 - T_\infty)Re_w \qquad (16)$$

is the characteristic temperature of the jet.

A parameter that describes the relative strength of inertia and buoyant forces is introduced here as

$$\zeta = (Re_w\, Re)^{1/3}/Gr^{1/5} \quad \text{for a free jet} \qquad (17a)$$

or

$$\zeta = (Re_w^2\, Re)^{1/4}/Gr^{1/5} \quad \text{for a wall jet.} \qquad (17b)$$

In terms of ζ, a dimensionless longitudinal coordinate can be defined as

$$\xi = (1+\zeta)^{-1} \qquad (18)$$

which also plays the role of a buoyancy parameter or mixed convection parameter. At the region near the slit nozzle ($x \to 0$), the buoyancy can be neglected and the system is nearly a pure momentum jet. In this case $Re \gg Gr$, therefore $\zeta \to \infty$ and $\xi = 0$. But at the downstream distance far from the nozzle, the buoyancy is dominant and the system behaves like a buoyant plume arising from a line thermal source. In this case, $\zeta \to 0$ and $\xi = 1$.

In addition to the dimensionless coordinates, a dimensionless stream function and a dimensionless temperature are respectively introduced as

$$f(\xi,\eta) = \psi/\nu\lambda \qquad (19)$$

and

$$\theta(\xi,\eta) = [(T-T_\infty)/T^*]\lambda. \qquad (20)$$

2.4. *Transformed equations of a plane free buoyant jet*

By using the dimensionless variables and coordinates defined in the above section, the system equations of a plane free buoyant jet can be transformed into the following forms:

$$f''' + \frac{5+4\xi}{15}ff'' + \frac{5-8\xi}{15}f'f' \pm \xi^5\theta = \frac{4}{15}\xi(1-\xi)\left(f'\frac{\partial f'}{\partial\xi} - f''\frac{\partial f}{\partial\xi}\right) \qquad (21)$$

$$Pr^{-1}\theta'' + \frac{5+4\xi}{15}(f\theta)' = \frac{4}{15}\xi(1-\xi)\left(f'\frac{\partial\theta}{\partial\xi} - \theta'\frac{\partial f}{\partial\xi}\right). \qquad (22)$$

The associated boundary conditions and integral constraints are

$$f(\xi,0) = 0, \quad f''(\xi,0) = 0, \quad \theta'(\xi,0) = 0 \qquad (23a\text{–}c)$$

$$f'(\xi,\infty) = 0, \quad \theta(\xi,\infty) = 0 \qquad (24)$$

$$(1-\xi)\frac{\mathrm{d}}{\mathrm{d}\xi}\left[\int_0^\infty f'f'\,\mathrm{d}\eta\right] + 3\int_0^\infty f'f'\,\mathrm{d}\eta = \frac{15}{4}\xi^4\int_0^\infty \theta\,\mathrm{d}\eta \qquad (25)$$

$$\lim_{\xi\to 0}\int_0^\infty f'f'\,\mathrm{d}\eta = 1/2 \qquad (26)$$

$$\int_0^\infty f'\theta\,\mathrm{d}\eta = 1/2. \qquad (27)$$

For the limiting cases of $\xi = 0$ and $\xi = 1$, equations (21)–(27) are readily reducible to the set of self-similar equations of a momentum free jet and a pure buoyant line plume, respectively.

2.5. *Transformed equations of a wall buoyant jet*

For the system of a wall buoyant jet, the presence of an adiabatic vertical wall causes slight changes in the transformed governing equations as well as the boundary conditions and constraints when compared

with the case of the free buoyant jet. In this case, equations (1)–(6) and (7b)–(9b) are transformed into

$$f''' + \frac{5+7\xi}{20} ff'' + \frac{5-7\xi}{10} f'f' \pm \xi^5\theta = \frac{7}{20}\xi(1-\xi)\left(f'\frac{\partial f'}{\partial \xi} - f''\frac{\partial f}{\partial \xi}\right) \quad (28)$$

$$Pr^{-1}\theta'' + \frac{5+7\xi}{20}(f\theta)' = \frac{7}{20}\xi(1-\xi)\left(f'\frac{\partial \theta}{\partial \xi} - \theta'\frac{\partial f}{\partial \xi}\right) \quad (29)$$

$$f(\xi,0) = 0, \quad f'(\xi,0) = 0, \quad \theta'(\xi,0) = 0 \quad (30)$$

$$f'(\xi,\infty) = 0, \quad \theta(\xi,\infty) = 0 \quad (31)$$

$$(1-\xi)\frac{\mathrm{d}}{\mathrm{d}\xi}\left[\int_0^\infty f'\left(\int_\eta^\infty f'f'\,\mathrm{d}\eta\right)\mathrm{d}\eta\right] + 4\int_0^\infty f'\left(\int_\eta^\infty f'f'\,\mathrm{d}\eta\right)\mathrm{d}\eta = \frac{20}{7}\int_0^\infty f'\left(\int_\eta^\infty \theta\,\mathrm{d}\eta\right)\mathrm{d}\eta \quad (32)$$

$$\lim_{\xi\to 0}\left[\int_0^\infty f'\left(\int_\eta^\infty f'f'\,\mathrm{d}\eta\right)\mathrm{d}\eta\right] = 1/2 \quad (33)$$

$$\int_0^\infty f'\theta\,\mathrm{d}\eta = 1. \quad (34)$$

By utilizing the boundary conditions, equations (32) and (33) can be further reduced into the following forms:

$$(1-\xi)\frac{\mathrm{d}}{\mathrm{d}\xi}\left[\int_0^\infty f(f')^2\,\mathrm{d}\eta\right] + 4\int_0^\infty f(f')^2\,\mathrm{d}\eta = \frac{20}{7}\int_0^\infty f\theta\,\mathrm{d}\eta \quad (35)$$

$$\lim_{\xi\to 0}\left[\int_0^\infty f(f')^2\,\mathrm{d}\eta\right] = 1/2. \quad (36)$$

Equations (28)–(31) and (34)–(36) are the universal formulation of a laminar wall buoyant jet. They can be readily reduced to the set of self-similar equations of a nonbuoyant wall jet ($\xi = 0$) and a buoyant wall plume ($\xi = 1$).

3. NUMERICAL METHOD

To obtain converged nontrivial solutions of the nonsimilar equations (21) and (22) subject to the boundary conditions (23) and (24) of zero values, additional conservation constraints should be satisfied simultaneously. Owing to the integral constraints, any standard finite-difference scheme cannot be applied directly. Therefore, we developed a numerical algorithm to deal with the integral constraints, which is then incorporated with Keller's box scheme [21]. To conserve space, we describe only the treatments of the integral constraints and boundary conditions.

3.1. *The discretization of the integral constraints*

For convenience, the two integral constraints (25) and (27) of the free buoyant jet are rewritten as

$$(1-\xi)\frac{\mathrm{d}F}{\mathrm{d}\xi} + 3F = \frac{15}{4}\xi^4 G \quad (37)$$

$$H = 1/2 \quad (38)$$

where

$$F = \int_0^\infty f'f'\,\mathrm{d}\eta, \quad G = \int_0^\infty \theta\,\mathrm{d}\eta$$

$$\text{and} \quad H = \int_0^\infty f'\theta\,\mathrm{d}\eta. \quad (39)$$

The initial condition of equation (37) is

$$\lim_{\xi\to 0} F = 1/2. \quad (40)$$

The net points are defined by

$$\eta_0 = 0, \quad \eta_j = \eta_{j-1} + h \quad j = 1,2,\ldots,J \quad (41)$$

$$\xi^0 = 0, \quad \xi^n = \xi^{n-1} + k \quad n = 1,2,\ldots,N \quad (42)$$

where the increments h and k can be uniform or nonuniform. Equations (37) and (38) can be discretized into the following finite-difference form by using central difference:

$$AF^n + BG^n + C = 0 \quad (43)$$

$$H^n = 1/2 \quad (44)$$

where

$$A = 1, \quad B = 0, \quad C = -1/2 \quad \text{for } n = 0 \quad (45)$$

and

$$A = (1-\xi^{n-1/2})/k + 3/2 \quad (46a)$$

$$B = -15(\xi^{n-1/2})^4/8 \quad (46b)$$

$$C = (3-A)F^{n-1} + BG^{n-1} \quad (46c)$$

for $n > 0$. In deriving the finite-difference equations (43) and (44), the following difference approximation was used for the derivative:

$$\mathrm{d}z/\mathrm{d}\xi = (z^n - z^{n-1})/k \quad (47)$$

and the middle point values were estimated by

$$z^{n-1/2} = (z^n + z^{n-1})/2 \quad (48)$$

where z is any function of ξ.

3.2. *Recurrence equations*

Trivial solutions or solutions not satisfying the integral constraints would be obtained if we solved the discrete governing equations associated only with the boundary conditions. To incorporate the additional two integral constraints with the conventional numerical scheme, our strategy is to drop the boundary conditions $f''(\xi,0) = 0$ and $\theta'(\xi,0) = 0$ and replace them with another two presupposed boundary conditions

$$f'(\xi,0) = s \quad \text{and} \quad \theta(\xi,0) = t \quad (49a,b)$$

where s and t are the guessed nonzero constants.

The equations (23a), (24) and (49a,b) will be used as boundary conditions to complete the system of difference equations. The two dropped boundary conditions $f''(\xi,0)=0$ and $\theta'(\xi,0)=0$, together with the two integral equations (43) and (44), are then treated as constraints. Once the converged solution of the difference equations is obtained, the refined values of s and t for the next trial can be estimated by the recurrence equations

$$s_{i+1}=s_i+\frac{D_2D_5-D_3D_4}{D_1D_3-D_2D_2} \tag{50a}$$

$$t_{i+1}=t_i+\frac{D_2D_4-D_1D_5}{D_1D_3-D_2D_2} \tag{50b}$$

where the subscript i denotes the ith iteration for adjusting the guessed boundary conditions, and

$$D_1=\sum_{m=1}^{4}a_m^2,\quad D_2=\sum_{m=1}^{4}a_mb_m,\quad D_3=\sum_{m=1}^{4}b_m^2$$
$$D_4=\sum_{m=1}^{4}a_mc_m,\quad D_5=\sum_{m=1}^{4}b_mc_m \tag{51}$$

where

$$a_1=\partial\theta'(\xi^n,0)_i/\partial s,\quad a_2=\partial f''(\xi^n,0)_i/\partial s$$
$$a_3=\partial H_i^n/\partial s,\quad a_4=A\frac{\partial F_i^n}{\partial s}+B\frac{\partial G_i^n}{\partial s}$$
$$b_1=\partial\theta'(\xi^n,0)_i/\partial t,\quad b_2=\partial f''(\xi^n,0)_i/\partial t$$
$$b_3=\partial H_i^n/\partial t,\quad b_4=A\frac{\partial F_i^n}{\partial t}+B\frac{\partial G_i^n}{\partial t}$$
$$c_1=\theta'(\xi^n,0)_i,\quad c_2=f''(\xi^n,0)_i$$
$$c_3=H_i^n-1/2,\quad c_4=AF_i^n+BG_i^n+C. \tag{52}$$

The above recurrence formulae are derived via the minimization of the sum of squares of the discrepancies for the constrained conditions. The derivatives involved in the recurrence formulae can be computed by solving two sets of linear systems called variational equations which were derived by taking the derivatives of the difference equations and boundary conditions with respect to s and t. These equations retain the tridiagonal block structure of the matrix, and hence can be solved efficiently by using Keller's scheme.

The iterations for adjusting the presupposed boundary conditions are repeated until the following criterion is achieved:

$$[f''(\xi^n,0)_i]^2+[\theta'(\xi^n,0)_i]^2+[H_i^n-1/2]^2+[AF_i^n+BG_i^n+C]^2\leqslant\varepsilon \tag{53}$$

where ε is a very small quantity, say, 10^{-8} or less. Whenever this criterion is satisfied, the unique solution which satisfies both the boundary conditions and integral constraints is surely obtained at ξ^n. Then, the computation procedures were shifted to the next marching step ξ^{n+1}.

For solving the system equation of a buoyant wall jet, similar procedures have been followed. However, the dropped boundary conditions for a wall jet should be $f'(\xi,0)=0$ and $\theta'(\xi,0)=0$, which were replaced by the presupposed boundary conditions $f''(\xi,0)=s$ and $\theta(\xi,0)=t$, respectively.

A uniform mesh size of $\Delta\xi=0.01$ and $\Delta\eta=0.05$ has been used, which gave convergent numerical results that do not change with further grid refinement. The edge of the boundary layer has been determined to be $\eta_\infty=18$ for a free jet and 25 for a wall jet.

4. RESULTS AND DISCUSSION

4.1. *Free buoyant jet*

Numerical results of $f'(\xi,0)$ and $\theta(\xi,0)$ for a free buoyant jet over the entire buoyancy region from a pure momentum jet ($\xi=0$) to a pure buoyant plume ($\xi=1$) are presented in Table 1 for $Pr=0.7$ and 7. Since the numerical calculations have been carried out step-by-step from $\xi=0$ to 1, the validity of the numerical results can be verified by comparing the results of $\xi=1$ with the reported data. As can be seen from Table 1, the present results of $\xi=1$ coincide excellently with the data converted from Fujji *et al.* [18]. In addition, the value of $f'(\xi,0)$ at $\xi=0$ is in excellent agreement with that of Wilks *et al.* [13].

4.1.1. *Velocity and temperature profiles of the free buoyant jet.* The typical dimensionless velocity

$$f'(\xi,\eta)=(u/u_0)Re\,\lambda^{-2} \tag{54}$$

and dimensionless temperature $\theta(\xi,\eta)$ of the free buoyant jet are presented in Figs. 1 and 2, respectively, for $Pr=0.7$. The evolution of the profiles from the limiting profile of a pure momentum jet ($\xi=0$) to that of a pure buoyant plume ($\xi=1$) can be seen from these figures. In addition, these figures also show that the profiles for different intensities of buoyancy are very similar. The similarity of the profiles indicates

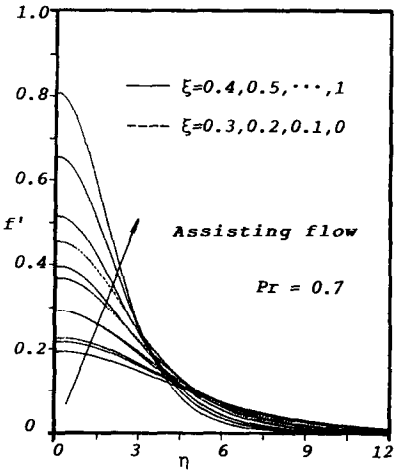

FIG. 1. Typical dimensionless velocity profiles $f'(\xi,\eta)$ of a free buoyant jet, $Pr=0.7$.

Table 1. Numerical results of $f'(\xi,0)$ and $\theta(\xi,0)$ of the free buoyant jet

	$f'(\xi,0)$		$\theta(\xi,0)$	
ξ	$Pr=0.7$	$Pr=7$	$Pr=0.7$	$Pr=7$
0	0.45428 [13]	0.45428 [13]		
0	0.45430	0.45430	0.41480	0.95116
0.1	0.36801	0.36802	0.46048	1.05689
0.2	0.29132	0.29146	0.51715	1.18862
0.3	0.22798	0.22952	0.58626	1.35251
0.4	0.19440	0.20237	0.65277	1.52762
0.5	0.21850	0.23653	0.66135	1.60529
0.6	0.29356	0.31801	0.60140	1.51338
0.7	0.39564	0.42644	0.52783	1.34710
0.8	0.51644	0.55530	0.46484	1.18855
0.9	0.65436	0.70245	0.41437	1.05753
1	0.80866	0.86713	0.37321	0.95150
1	0.80872†		0.37328†	

† Data converted from Fujji *et al.* [18].

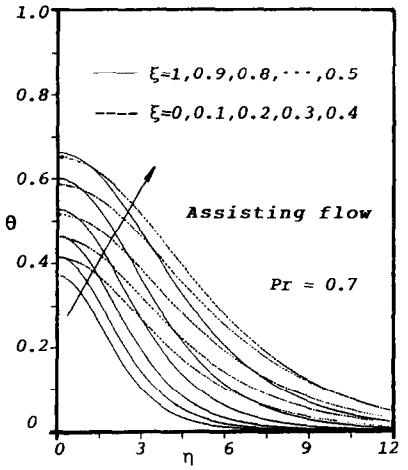

FIG. 2. Typical dimensionless temperature profiles $\theta(\xi,\eta)$ of a free buoyant jet, $Pr=0.7$.

that the present dimensionless variables and coordinates are very appropriate for the analyses of the buoyant jets.

Figures 1 and 2 have been recast into Figs. 3 and 4 which are more explicit in a physical sense. In these figures, we plot the dimensionless longitudinal velocity

$$U=(u/u_0)(Re_w^2/Gr_w)^{1/4}=\zeta^{-3/4}\xi^{-2}f'(\xi,\eta) \quad (55)$$

and the dimensionless temperature

$$\varphi=[(T-T_\infty)/T^*](Re_w^6/Gr_w)^{1/4}=\zeta^{9/4}\xi\theta(\xi,\eta) \quad (56)$$

versus the dimensionless transverse coordinate

$$Y=(y/w)(Gr_w^2/Re_w^4)^{1/4}=\zeta^{-6/4}\xi\eta. \quad (57)$$

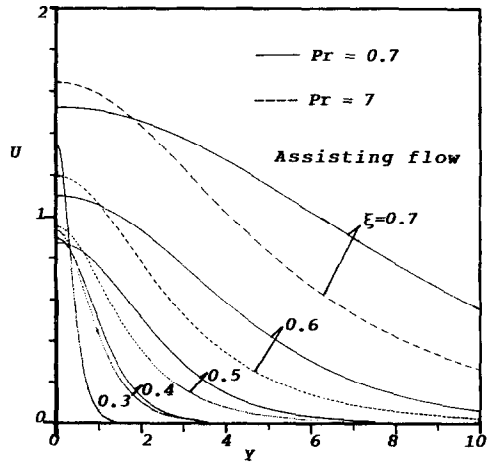

FIG. 3. Profiles of the dimensionless velocity U of a free buoyant jet, $Pr=0.7$.

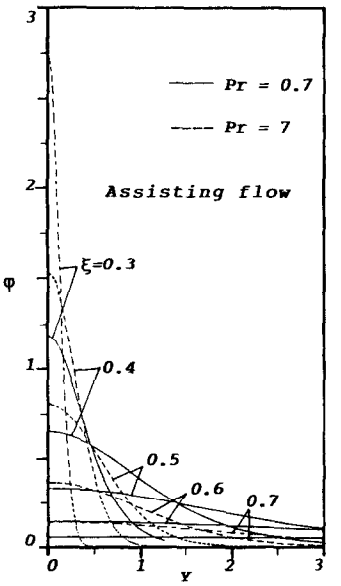

FIG. 4. Profiles of the dimensionless temperature φ of a free buoyant jet, $Pr=0.7$.

The downstream distance x has thus been eliminated from the dimensionless variables U, φ, and Y, and is contained only in the mixed convection parameter ξ. Figures 3 and 4 show that the dimensionless velocity and temperature profiles develop from the sharp and narrow ones of the jet type to the flattened and wide ones of the plume type as the buoyancy parameter ξ increases.

4.1.2. *Variations of the centerline velocity and centerline temperature of the free buoyant jet.* The variations of the dimensionless centerline velocity $U_c = (u_c/u_0)(Re_w^2/Gr_w)^{1/4}$ with respect to the dimensionless downstream distance

$$X = (x/w)(Gr_w^3/Re_w^{10})^{1/4} = \zeta^{-15/4} \qquad (58)$$

are shown in Fig. 5 for fluids of $Pr = 0.7$ and 7. This figure shows that the centerline velocity initially decreases with downstream distance from the slit, then reaches a minimum and thereafter increases steadily. This figure reveals a deceleration region near the slit and an acceleration region at a downstream distance far from the slit. At the deceleration region the centerline velocity of the free buoyant jet is retarded by the viscous force and decreases to a minimum. At the acceleration region, the buoyancy force increases and drives the fluid to flow faster.

The variations of the centerline temperature φ_c with the dimensionless longitudinal distance X are presented in Fig. 6. This figure shows that the centerline temperature decreases monotonically with increasing downstream distance. Further inspection of this figure reveals that there are two different slopes corresponding to the jet region and the plume region. The region of transition from the momentum jet to the buoyant plume is around $X = 0.5$, as indicated in Figs. 5 and 6. These figures also indicate that the centerline velocity and centerline temperature of $Pr = 7$ are higher than those of $Pr = 0.7$.

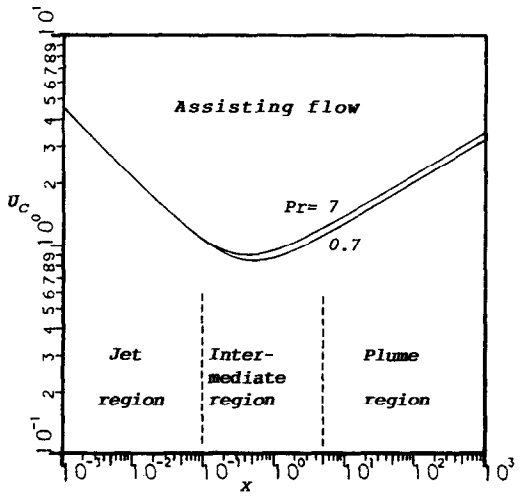

FIG. 5. The variations of the dimensionless centerline velocity U_c of a free buoyant jet, $Pr = 0.7$ and 7.

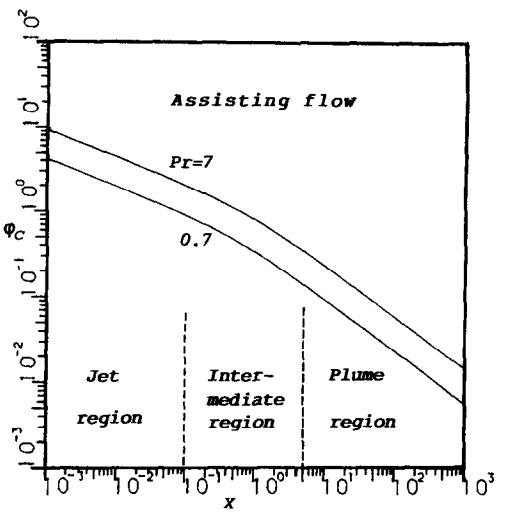

FIG. 6. The variations of the dimensionless centerline temperature φ_c of a free buoyant jet, $Pr = 0.7$ and 7.

4.1.3. *Correlation equations of the centerline temperature and centerline velocity.* For application convenience, we propose a simple but very accurate correlation equation

$$[1/\theta(\xi,0)]^m = [(1-\xi)/\theta(0,0)]^m \pm [\xi/\theta(1,0)]^m \qquad (59)$$

for the prediction of the centerline temperature of the free buoyant jet at any downstream distance. The plus and minus signs in front of the last term of equation (59) refer to the buoyancy assisting and opposing flows, respectively. The values of $\theta(0, 0)$ and $\theta(1, 0)$ for the limiting cases of a momentum jet ($\xi = 0$) and a buoyant plume ($\xi = 1$), respectively, are listed in Table 1. The positive constant m will be specified to minimize the discrepancy between the correlation and the numerical data. For $m = 4$, the discrepancy is less than 0.9% over the entire region of buoyancy ($0 \leqslant \xi \leqslant 1$) for $Pr = 0.7$ and 7. The maximum discrepancy occurs in the transition region ($0.4 < \xi < 0.5$).

The centerline velocity can be predicted by the proposed correlation equation

$$[f'(\xi,0)]^m = [f'(0,0)]^m(1-\xi)^{2m} \pm [f'(1,0)]^m \xi^{2m}. \qquad (60)$$

The values of $f'(0,0)$ and $f'(1,0)$ for the limiting cases are presented in Table 1. The maximum error of the correlation equation with $m = 2.5$ is less than 0.7% for $Pr = 0.7$ and 1.5% for $Pr = 7$ over the whole range of buoyancy ($0 \leqslant \xi \leqslant 1$).

4.2. *Wall buoyant jet*

Numerical results of $f'(\xi, 0)$ and $\theta(\xi, 0)$ for a wall buoyant jet over the entire buoyancy assisting flow region from a momentum wall jet ($\xi = 0$) to a buoyant wall plume ($\xi = 1$) are presented in Table 2 for $Pr = 0.7$ and 7. The results of the buoyancy opposing flow are also listed in this table. The validity of the

Table 2. Numerical results of $f''(\xi,0)$ and $\theta(\xi,0)$ of the wall buoyant jet

	$f''(\xi,0)$		$\theta(\xi,0)$	
ξ	$Pr=0.7$	$Pr=7$	$Pr=0.7$	$Pr=7$
Assisting flow				
0	0.131353†	0.131353†		
0	0.13134	0.13134	0.70157	2.06556
0.1	0.09579	0.09581	0.77927	2.29488
0.2	0.06810	0.06914	0.87620	2.57958
0.3	0.05303	0.06217	0.99610	2.91774
0.4	0.06582	0.09867	1.12017	3.21977
0.5	0.12022	0.19139	1.16954	3.33478
0.6	0.21404	0.34264	1.10343	3.22464
0.7	0.34509	0.55567	0.99040	2.96772
0.8	0.51790	0.83642	0.88003	2.66634
0.9	0.73887	1.19327	0.78596	2.38529
1	1.01495	1.63932	0.70813	2.15625
1	1.01493 [20]		0.70815‡	
Opposing flow				
0	0.13134	0.13134	0.70157	2.06556
0.05	0.11263	0.11263	0.73835	2.17416
0.1	0.09575	0.09572	0.77928	2.29495
0.15	0.08050	0.08028	0.82509	2.43024
0.20	0.06642	0.06535	0.87687	2.58389
0.25	0.05247	0.04860	0.93645	2.76383
0.30	0.03633	0.02296	1.00766	2.99264

† Exact solution converted from ref. [16].
‡ Data converted from Liburdy and Faeth [20].

numerical results has been verified in Table 2 by comparing with the exact solution of $f''(0,0)$ converted from ref. [16], and with the data of $f''(1,0)$ and $\theta(1,0)$ converted from Liburdy and Faeth [20] for the wall plume.

4.2.1. *Velocity and temperature profiles of the wall buoyant jet.* For a jet propagating along an adiabatic plane wall, the typical profiles of the dimensionless velocity $f'(\xi,\eta)=(u/u_0)Re\,\lambda^{-2}$ and the dimensionless temperature $\theta(\xi,\eta)$ are presented in Figs. 7 and 8, respectively. Another dimensionless longitudinal velocity

$$U=(u/u_0)(Re_w^2/Gr_w)^{1/7}=\zeta^{-4/7}\xi^{-2}f'(\xi,\eta) \quad (61)$$

over the dimensionless transverse coordinate

$$Y=(y/w)(Gr_w^3/Re_w^6)^{1/7}=\zeta^{-8/7}\xi\eta \quad (62)$$

is shown in Fig. 9, while the profiles of the dimensionless temperature

$$\varphi=[(T-T_\infty)/T^*](Re_w^9/Gr_w)^{1/7}=\zeta^{12/7}\xi\theta(\xi,\eta) \quad (63)$$

over Y are presented in Fig. 10. The profiles are sharp and high in the jet region of small ξ, whereas the profiles are flatter and low in the plume region of large ξ where the jet fluid is spread wider.

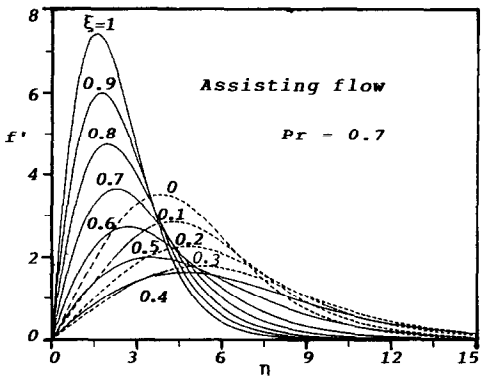

FIG. 7. Typical dimensionless velocity profiles $f'(\xi,\eta)$ of a wall buoyant jet, $Pr=0.7$.

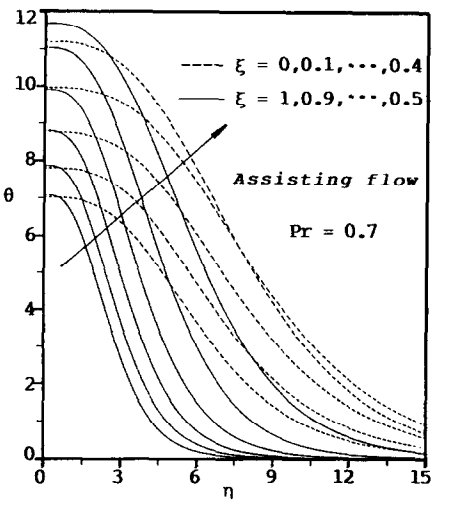

FIG. 8. Typical dimensionless temperature profiles $\theta(\xi,\eta)$ of a wall buoyant jet, $Pr=0.7$.

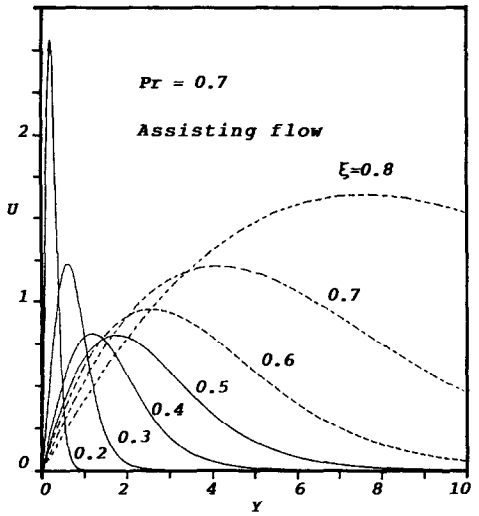

FIG. 9. Profiles of the dimensionless velocity U of a wall buoyant jet, $Pr = 0.7$.

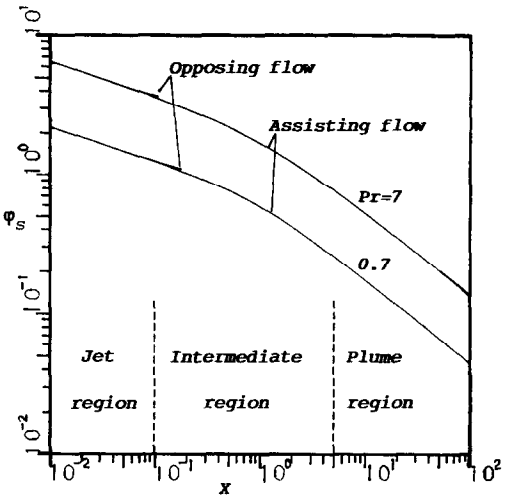

FIG. 11. The variations of the dimensionless surface temperature φ_s of a wall buoyant jet, $Pr = 0.7$ and 7.

4.2.2. *Variations of the surface temperature and shear stress.* For the wall buoyant jets, the most interesting physical quantity is the variation of the surface temperature. Figure 11 shows the dimensionless temperature $\varphi_s = [(T_s - T_\infty)/T^*](Re_w^9/Gr_w)^{1/7}$ versus the dimensionless distance

$$X = (x/w)(Gr_w^4/Re_w^{15})^{1/7} = \zeta^{-20/7}. \quad (64)$$

This figure shows the decay of surface temperature along the downstream distance. It also displays the jet region ($X < 0.1$), the intermediate region ($0.1 < X < 5$), and the plume region ($X > 5$).

Another physical quantity of interest is the shear stress at the surface, which can be expressed in dimensionless form as

$$C_f = \tau_s/\rho(\nu/x)^2 = \lambda^3 f''(\xi, 0) \quad (65)$$

or as

$$C_f/(Re_w^{1/2}Re^{1/4})^3 = (1-\xi)^{-3} f''(\xi, 0). \quad (66)$$

A plot of $C_f/(Re_w^{1/2}Re^{1/4})^3$ versus ζ is shown in Fig. 12 for both the buoyancy assisting and opposing flows. The values of $C_f/(Re_w^{1/2}Re^{1/4})^3$ attain nearly a constant of 0.13134 for $\zeta < 0.2$. The surface friction increases with increasing buoyancy parameter ζ for the case of buoyancy assisting flow but decreases with increasing ζ for buoyancy opposing flow. An alternative expression of the variation of surface shear stress along the downstream distance is presented in Fig. 13. In this figure, the dimensionless surface shear stress is defined as

$$[\tau_s/\rho(\nu/w)^2](Re_w^3/Gr_w^5)^{1/7} = \zeta^{4/7}\xi^{-3} f''(\xi, 0). \quad (67)$$

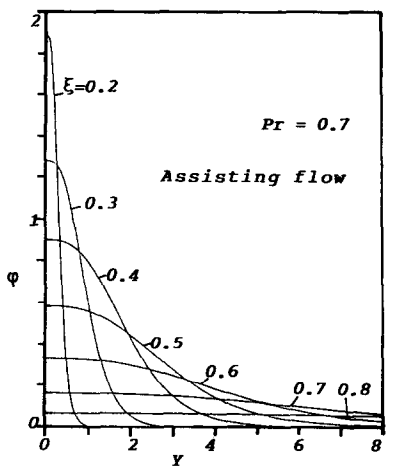

FIG. 10. Profiles of the dimensionless temperature φ of a wall buoyant jet, $Pr = 0.7$.

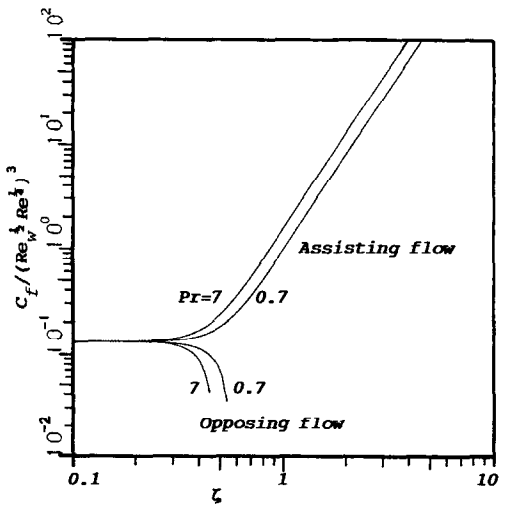

FIG. 12. The variations of the friction coefficient $C_f/(Re_w^{1/2}Re^{1/4})^3$ of a wall buoyant jet, $Pr = 0.7$ and 7.

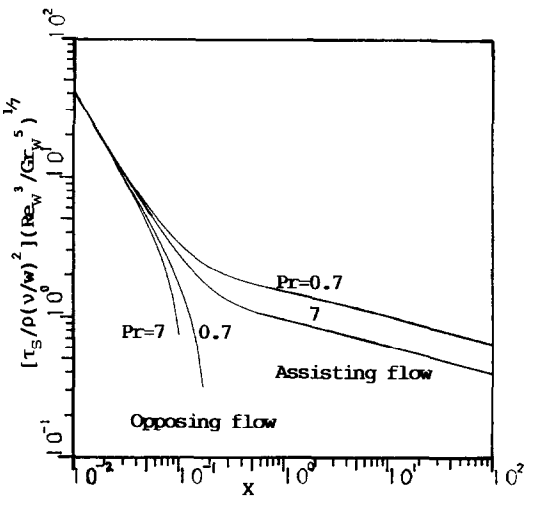

FIG. 13. The variations of the dimensionless surface shear stress $[\tau_s/\rho(\nu/w)^2](Re_w^3/Gr_w^5)^{1/7}$ of a wall buoyant jet, $Pr = 0.7$ and 7.

4.2.3. *Correlation equations of the surface temperature and the surface shear stress of the wall buoyant jet.* The correlation equation of the surface temperature for the wall buoyant jet is the same as that of the centerline temperature for the free buoyant jet. The values of $\theta(0,0)$ and $\theta(1,0)$ for the limiting cases of the pure wall jet ($\xi = 0$) and the pure wall plume ($\xi = 1$) are presented in Table 2. For the buoyancy assisting flow over the whole buoyancy region ($0 \leqslant \xi \leqslant 1$), the maximum error of the correlation equation with $m = 4$ is less than 2.1% for $Pr = 0.7$ and 5.8% for $Pr = 7$. For the buoyancy opposing flow over the region of $0 < \xi < 0.3$, the maximum error is less than 0.3% for $Pr = 0.7$ and 0.7% for $Pr = 7$. The maximum error of the correlation for the buoyancy assisting flow of $Pr = 7$ can be reduced from 5.8 to 1.2% if $m = 4$ is replaced by $m = 3$.

The surface shear stress can be predicted by the proposed correlation equation of $f''(\xi,0)$:

$$[f''(\xi,0)]^m = [f''(0,0)]^m(1-\xi)^{3m} \pm [f''(1,0)]^m \xi^{3m}. \tag{68}$$

The values of $f''(0,0)$ and $f''(1,0)$ for the limiting cases of $\xi = 0$ and $\xi = 1$ are listed in Table 2. For $Pr = 0.7$, the maximum error of the correlation equation with $m = 4$ is less than 5.5% over the range of $0 \leqslant \xi \leqslant 1$ for the buoyancy assisting flow and 1.6% over $0 < \xi < 0.3$ for the buoyancy opposing flow. For $Pr = 7$, the maximum error of the correlation equation with $m = 3$ is less than 7.1% for the buoyancy assisting flow.

5. CONCLUSIONS

In this paper, we have introduced some dimensionless variables and parameters of proper scales for the analyses of the two-dimensional laminar free buoyant jet and the wall buoyant jet. Universal formulations, valid uniformly over the entire buoyancy region from pure momentum jets to pure buoyant plumes, are obtained. To solve the transformed nonsimilar equations subject to the integral constraints of momentum and heat flux conservations, we have developed an effective numerical scheme and obtained very accurate solutions. The characteristics of the buoyant jets as a combination of the momentum jets and the buoyant plumes were clearly shown in the figures. Very accurate correlation equations of the centerline velocity and the centerline temperature of the free buoyant jet have been proposed. The correlations of the surface shear stress and the surface temperature of the wall buoyant jet have also been introduced.

Since the analysis is based on the boundary layer approximation, only the buoyancy assisting jet and the buoyancy opposing jet with slight negative buoyancy can be studied by the proposed method. A breakdown in the numerical integration occurs as the negative buoyancy increases to a critical value (e.g. $\xi \approx 0.31$ for the case of the buoyancy opposing wall jet). The slight negative buoyancy will not reverse the jet flow but only retards it. The jet with reverse flow is beyond the scope of this paper. In addition, the present conventional method cannot deal with the large scale motions at the outer edge of the boundary layer. Nevertheless, the present method of analysis and the developed numerical scheme as well as the forms of the correlations can be applied to many other jets.

Acknowledgement—The support of this work by the National Science Council of the Republic of China is gratefully acknowledged (Grant No. NSC78-0402-E008-10).

REFERENCES

1. H. Schlichting, Laminare strahlausbreitung, *Z. Angew. Math. Mech.* **13,** 260 (1933).
2. W. Bickley, The plane jet, *Phil. Mag.* **23,** 727–731 (1939).
3. M. B. Glauert, The wall jet, *J. Fluid Mech.* **1,** 625–642 (1956).
4. L. A. Vulis and A. T. Trofimenko, Thermal problems for a laminar jet propagating along a wall, *Zh. Tekh. Fiz.* **26,** 2709–2713 (1956).
5. W. H. Schwarz and B. Caswell, Some heat transfer characteristics of the two-dimensional laminar incompressible wall jet, *Chem. Engng Sci.* **16,** 338–351 (1961).
6. R. S. Brand and F. J. Lahey, The heated laminar vertical jet, *J. Fluid Mech.* **29,** 305–315 (1967).
7. S. B. Savage and G. K. C. Chan, The buoyant two-dimensional laminar vertical jets, *Q. J. Mech. Appl. Math.* **23,** 413–430 (1970).
8. J. C. Mollendorf and B. Gebhart, Thermal buoyancy in round laminar vertical jets, *Int. J. Heat Mass Transfer* **16,** 735–745 (1973).
9. J. W. Yang and R. D. Patel, Effect of buoyancy on forced convection in a two-dimensional wall jet along a vertical wall, *J. Heat Transfer* **95,** 121–123 (1973).
10. R. S. R. Gorla, Combined natural and forced convection in a laminar wall jet along a vertical plate with uniform surface heat flux, *Appl. Scient. Res.* **31,** 455–465 (1976).
11. J. L. Bansal and S. S. Tak, Approximate solutions of heat and momentum transfer in laminar plane wall jet, *Appl. Scient. Res.* **34,** 299–311 (1978).
12. W. Schneider and K. Potsch, Weak buoyancy in laminar vertical jets. In *Review of the Developments in Theoretical*

and Experimental Fluid Mechanics (Edited by U. Muller *et al.*), pp. 501–510. Springer, Berlin (1979).
13. G. Wilks, R. Hunt and D. S. Riley, The two-dimensional laminar vertical jet with positive or adverse buoyancy, *Numer. Heat Transfer* **8**, 449–468 (1985).
14. Y. Jaluria, Hydrodynamics of laminar buoyant jets. In *Encyclopedia of Fluid Mechanics* (Edited by N. P. Cheremsinoff), Vol. 2, pp. 317–348. Gulf, Houston, Texas (1986).
15. O. G. Martynenko, V. N. Korovkin and Yu. A. Sokovishin, The class of self-similar solutions for laminar buoyant jets, *Int. J. Heat Mass Transfer* **32**, 2297–2307 (1989).
16. P.-C. Lu, *Introduction to the Mechanics of Viscous Fluids*. Holt, Rinehart & Winston, New York (1976).
17. H. Schlichting, *Boundary Layer Theory* (7th Edn), p. 180. McGraw-Hill, New York (1979).
18. T. Fujji, I. Morioka and H. Uehara, Buoyant plume above a horizontal line heat source, *Int. J. Heat Mass Transfer* **16**, 755–768 (1973).
19. Y. Jaluria and B. Gebhart, Buoyancy induced flow arising from a line thermal source on an adiabatic vertical surface, *Int. J. Heat Mass Transfer* **20**, 153–157 (1977).
20. J. A. Liburdy and G. M. Faeth, Theory of a steady laminar thermal plume along a vertical adiabatic wall, *Lett. Heat Mass Transfer* **2**, 407–418 (1975).
21. H. B. Keller, Numerical methods in boundary-layer theory, *A. Rev. Fluid Mech.* **10**, 417–433 (1978).

SOLUTIONS NUMERIQUES RIGOUREUSES ET FORMULES POUR LES JETS FLOTTANTS LAMINAIRES BIDIMENSIONNELS

Résumé—On propose une méthode de résolution très efficace et précise pour traiter les jets libres et flottants pariétaux. Les jets flottants sont considérés comme une combinaison de jets de quantité de mouvement et de panaches flottants, et ils sont analysés en introduisant quelques variables sans dimension, dans le domaine complet du flottement. Un schéma efficace et rigoureux aux différences finies est développé pour résoudre les équations non similaires. Des formules précises sont proposées pour prédire la température et la vitesse sur la ligne centrale des jets flottants libres, laminaires et bidimensionnels. On présente aussi des formules pour la température et le frottement en surface pour les jets pariétaux flottants.

NUMERISCHE LÖSUNG UND KORRELATION FÜR EINEN ZWEIDIMENSIONALEN LAMINAREN AUFTRIEBSSTRAHL

Zusammenfassung—Für die Untersuchung freier und wandanliegender Auftriebsstrahlen wird ein sehr wirksames und genaues Lösungsverfahren vorgeschlagen. Die Auftriebsstrahlen werden als kombiniertes System aus Impulsstrahlen und Auftriebsfahnen behandelt. Bei der Analyse werden einige geeignete dimensionslose Kennzahlen für den gesamten Auftriebsbereich angewandt. Zur Lösung der nichtähnlichen Gleichungen für die Impuls- und Energieerhaltung wird ein wirksames Finite-Differenzen-Verfahren entwickelt. Zur Beschreibung von Temperatur und Geschwindigkeit in der Symmetrielinie eines zweidimensionalen laminaren freien Auftriebsstrahls werden sehr genaue Korrelationsgleichungen vorgeschlagen. Außerdem werden Korrelationsgleichungen für die Oberflächentemperatur und die Schubspannung an der Oberfläche wandanliegender Auftreibsstrahlen vorgelegt.

ТОЧНЫЕ ЧИСЛЕННЫЕ РЕШЕНИЯ И СООТНОШЕНИЯ ДЛЯ РАСЧЕТА ДВУМЕРНЫХ ЛАМИНАРНЫХ СВОБОДНОКОНВЕКТИВНЫХ СТРУЙ

Аннотация—Предложен весьма эффективный и точный метод исследования свободных и пристенных свободноконвективных струй. Свободноконвективная струя рассматривается как комбинированная система, состоящая из динамических и плавучих струй, которые анализируются путем введения некоторых безразмерных переменных соответствующих масштабов во всем диапазоне действия подъемной силы. Разработана эффективная и точная схема конечных разностей для решения неавтомодельных уравнений с соответствующими интегральными ограничениями сохранения момента и теплового потока. Предложены очень точные обобщающие соотношения для расчета температуры и скорости на центральной линии двумерных ламинарных свободных плавучих струй. Также представлены корреляции между температурой поверхности и напряжения трения плавучих пристенных струй.